Benchmarking DFT functionals for photophysics of pyranoflavylium cations

JHONATHAN R. SOUZA[1,3,4]; CARLES CURUTCHET[3,4]; YURI A. AOTO[2]; PAULA HOMEM-DE-MELLO[1*]

1. Centro de Ciências Naturais e Humanas (CCNH), Universidade Federal do ABC (UFABC), Avenida dos Estados 5001, 09210-580, Santo André, São Paulo, Brasil.
2. Centro de Matemática, Computação e Cognição (CMCC), Universidade Federal do ABC (UFABC), Avenida dos Estados 5001, 09210-580, Santo André, São Paulo, Brasil.
3. Departament de Farmàcia i Tecnologia Farmacèutica, i Fisicoquímica, Facultat de Farmàcia i Ciències de l'Alimentació, Universitat de Barcelona (UB), Av. Joan XXIII 27-31, 08028, Barcelona, Espanya.
4. Institut de Química Teòrica i Computacional (IQTC), Universitat de Barcelona (UB), Martí i Franques, 1, 08028, Barcelona, Espanya.
* Corresponding author: paulahmello@gmail.com / paula.mello@ufabc.edu.br

KEYWORDS: Electronic Structure, Photophysics, Excited-states, Time-dependent Density Functional Theory (TD-DFT), Benchmark, Photosensitizers

ABSTRACT

An intense absorption, phosphorescence, a long triplet excited state lifetime and singlet oxygen generation capabilities are characteristics of pyranoflavylium cations, analogues to pyranoanthocyanidins originated in the maturation process of red wine. Such properties make these compounds potential photosensitizers to be applied in photodynamic therapy. In this context, the photophysical processes underlying that treatment critically depend on the electronic structure of the pyranoflavylium molecules. When employing density functional theory to describe the electronic structure of molecules, the choice of the most suitable functional is not trivial, and benchmark studies are needed to orient practitioners in the field. In this work, a benchmark of seven of the most commonly used density functionals in addressing the photophysical properties of a set of eight pyranoflavylium cations is reported. Ground and excited state geometries, molecular orbitals, and absorption, fluorescence and phosphorescence transition energies were calculated using density functional theory approaches, and evaluated and compared to experimental data and monoreferential wave function-based methodologies. Statistical analysis of the results indicates that global-hybrid functionals allow an excellent

description of absorption and emission energies, with errors around 0.05 eV, while range-separated variants led to somewhat larger errors in the range 0.1-0.2 eV. In contrast, range-separated functionals display excellent phosphorescence energies with errors close to 0.05 eV, in this case global-hybrids showing increased discrepancies around 0.5-0.1 eV.

INTRODUCTION

Recent studies have demonstrated that pyranoflavylium cations (PF^+), compounds analogues to pyranoanthocyanidins originated in red wine, show interesting spectroscopic features to perform as photosensitizers.[1,2] Intense absorption bands at UV-visible spectral range and a triplet excited state with a long lifetime are the main characteristics that turn these molecules into potential photosensitizers, for instance, to be used in photodynamic therapy (PDT).[3,4] In this context, a correct description of their electronic structure can help not only understanding their photophysical properties, but also in designing new and more efficient photosensitizers.

The molecular photosensitization phenomenon starts with light absorption and ends when the ground-state is reached again, what can happen through different decaying processes.[5,6] Although some higher singlet excited states are populated in response to photoabsorption, in general, following Kasha's rule, the electronic structure relaxes to the first singlet excited state (S_1), from which important processes can take place, for example, fluorescence and intersystem crossing.[7] In the case of photodynamic therapy, the first triplet excited state (T_1) properties, such as the phosphorescence energy, are also relevant, given that electron and energy transfer processes involving this state are responsible for the effectiveness of the treatment.[8–12]

Nowadays, time-dependent density functional theory (TD-DFT) has emerged as a powerful tool to describe molecular electronic structure and excited states properties, presenting an excellent balance in terms of accuracy and computational cost.[13–19] TD-DFT approaches allow to characterize molecular geometries and simulate single excitations, thus providing access to important spectral features, for example, the absorption and emission energies, and the molecular orbital contributions to electronic transitions.[20–24] However, choosing the most suitable density functional to simulate molecular properties is not a trivial task, given the myriad of options developed in the last decades, which motivate the need for detailed benchmarking studies aimed at guiding

practitioners in such choices.[25–29] In the present study, the ability of different density approaches to simulate the photophysical properties of PF^+ photosensitizers have been assessed. So far, global-hybrid (GH) and range-separated (RS) functionals are the most popular choice when dealing with molecular excited states. This is partly due to their widespread availability in quantum chemistry software, but mainly because they lead to accurate results when benchmarked with experimental data and wave function approaches.[30–33] GH functionals are generally built based on the meta-generalized gradient approximation, in which electronic density, electronic density gradient and electronic density kinetic energy are the main variables.[34,35] At the same time, a percentage (α) of Hartree-Fock exchange (E_x^{HF}) is also considered when calculating the exchange-correlation energy,[36,37] as expressed in Equation 1.

$$E_{xc}^{GH} = \alpha E_x^{HF} + (1-\alpha)E_x^{DFT} + E_c^{DFT} \quad (1)$$

The value α can be set based on theoretical arguments, but it is more frequent to determine that by fitting to training datasets. Depending on the desired property, the optimal value for α can drastically vary. For instance, one of the most employed functionals, B3LYP, has a percentage of Hartree-Fock exchange of 20%, TPSSh of 10%, B98 of 22%, and PBE0 of 25%. In the case of the M06 functional, the percentage is 27% - the authors claim it is adequate to describe organometallic chemistry and noncovalent interactions – and for the M06-2X, the percentage is 54%, and it is recommended for main-group thermochemistry, and Rydberg states energies.[34]

The range-separated functionals share the same essence as hybrid functionals, but in this strategy, a parameter ω was proposed to define the HF exchange ratio over the distance.[38,39] The two-electrons coulombic repulsion term is decomposed as expressed in Equation (2).

$$\frac{1}{r_{12}} = \frac{erf\,(\omega r_{12})}{r_{12}} + \frac{erfc(\omega r_{12})}{r_{12}} \quad (2)$$

$$E_{xc}^{RS} = pE_x^{HF} + (1-p)(E_x^{LR-HF} + E_x^{SR-DFT}) + E_c^{DFT} \quad (3)$$

Such separation leads to a HF exchange acting in long-range distances while DFT exchange acts over short-range distances, as written in Equation (3). It is also possible to

tune the omega value to reproduce some target properties better. However, in this work, we chose to keep the default values of the software to compare with the default parameters of the other functionals.

In order to provide a comprehensive picture of radiative photophysical processes while benchmarking different density functionals, in this work the electronic structure of eight pyranoflavylium cation (PF1-PF8 in Figure 1) was calculated by means of TD-DFT methods. Molecular orbitals, excited states diagrams and electronic transitions were scrutinized. In addition, solvatochromic effects on PF^+ properties were also investigated through the IEF-PCM continuum solvation model. Finally, DFT results were also compared to the single-reference wave function method second-order Moller-Plesset perturbation theory (MP2) and second-order algebraic diagrammatic construction (ADC(2)) together with the conductor-like screening solvation model (COSMO).[40]

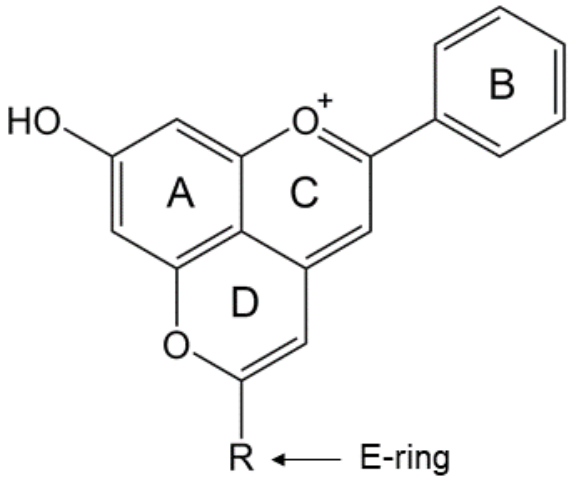

PF1: R = p-methoxyphenyl
PF2: R = p-methylphenyl
PF3: R = 2-naphthyl
PF4: R = phenyl
PF5: R = p-fluorphenyl
PF6: R = m-pyridyl
PF7: R = p-cyanophenyl
PF8: R = p-nitrophenyl

Figure 1: Pyranoflavylium cations investigated in this work. R group is also referred as E ring along the text

COMPUTATIONAL DETAILS

The software Gaussian09[41] was employed for all density functional theory calculations reported in this work. Optimized geometries for ground (S_0), and excited (S_1 and T_1) states were calculated using the functionals TPSSh[36], B3LYP[42], B98[43], PBE0[44], M06[34], CAM-B3LYP[45] and ωB97XD[46], with default α and ω parameters, together with the split-valence gaussian basis set 6-311++G(d,p). To compare theoretical results to experimental data, the ground state and excited states geometries were also optimized in

implicit solvent. The IEF-PCM method[48–52] with Gaussian09 default settings was employed to simulate acetonitrile and isopropanol solutions.

The electronic absorption spectra were obtained by computing up to thirty (30) singlet excited states, both in gas phase and in acetonitrile, the latter being the solvent used to measure the experimental photoabsorption spectrum. On the other hand, the emission phenomena were measured in isopropanol solvent.[4] Thus, the geometries of the S_1 and T_1 excited states were also obtained in gas and isopropanol solution. The vertical fluorescence ($S_1 \rightarrow S_0$) and vertical phosphorescence ($T_1 \rightarrow S_0$) emissions were calculated using all functionals previously described. To do so, the fluorescence energies were estimated as the energy difference between the optimized molecular conformation of the first singlet excited state (S_1) and the ground-state energy for this same geometry. The TPSSh functional is not available for excited state geometry optimizations by means of TD-DFT in the Gaussian09 software version employed. The phosphorescence energies were calculated in the same way as it was done for fluorescence but considering the first triplet excited state optimized geometry. For punctual cases for PF7 and PF8 compounds, diffuse functions led to convergence problems, and the 6-311G(d,p) basis set[47] was used instead (Figures SI21 – SI23).

The present benchmark includes a statistical analysis, in which averaged energies, relative errors and standard deviation are reported for the results based on global-hybrid and range-separated functionals. They were calculated for the photophysical processes under investigation, namely absorption to the S_1 and emissions from the S_1 and T_1 states.

RESULTS AND DISCUSSION

Geometries

The absence of imaginary frequencies in the Hessian matrix for gas-phase and solvated phases indicated that all obtained geometries correspond to a minimum energy conformation. When comparing the cartesian coordinates among DFT functionals and between the electronic states S_0, S_1 and T_1, the dihedral angles defined by the C-B and D-E rings were found to display the greatest conformational discrepancies. In Figures SI1, SI2 and SI3 (support information), it is possible to appreciate both C-B and D-E optimal dihedral angles as a function of the DFT functional employed in gas-phase, in acetonitrile and in isopropanol, respectively.

In general, optimal dihedral angle values provided by the DFT methods show good agreement among themselves for all pyranoflavylium cations, both in gas-phase and in solution. However, for PF1 and PF3, gas-phase calculations based on global-hybrid methods lead to D-E dihedral angles around 90°. The inclusion of solvent effects largely mitigates these discrepancies, which suggests that solvation could yield more consistent results than gas-phase simulations when benchmarking DFT methods.

Overall, the B-C and D-E dihedral angles present different trends for each electronic state. For example, acute angles ($0°<\theta<30°$) are found for the ground-state. However, for the S_1 and T_1 states, except when the ωB97XD functional is used, the B-C and D-E rings define dihedral angles close to 0°, which provides a flat conformation for all molecules. Such different conformations for different excited states suggest that both radiative and non-radiative decay processes could be related to specific B and E ring torsions. Besides, once the vertical emission processes start from the relaxed geometry of the excited state, the similar conformation for both S_1 and T_1 suggests that the spectrum emission profiles for both fluorescence and phosphorescence could present similar vibrational couplings in spectral measurements, as it was observed in experimental data[53].

Table 1: Ground-state D-E dihedral angles (°) calculated by MP2 and DFT methods for PF^+ compounds

Gas-phase								
Molecule	**MP2[a]**	**TPSSh**	**B3LYP**	**B98**	**PBE0**	**M06**	**CAM**	**ωB97XD**
PF1	18.4	1.1	1.1	1.5	1.8	1.8	5.7	14.6
PF2	22.1	1.7	1.4	4.1	12.3	1.9	16.4	18.7
PF3	-	12.7	15.8	16.8	16.8	17.0	19.5	23.2
PF4	26.2	15.5	17.4	18.4	18.5	16.8	20.3	25.1
PF5	23.8	7.6	15.6	15.9	16.3	3.4	18.8	21.0
PF6	-	18.9	20.1	20.9	20.6	19.1	22.0	27.8
PF7	23.3	15.8	19.3	20.1	19.8	20.1	22.1	26.0
PF8	25.6	18.3	21.1	21.7	21.7	21.7	23.8	27.7
Acetonitrile								
Molecule	**B3LYP[a]**	**TPSSh**	**B3LYP**	**B98**	**PBE0**	**M06**	**CAM**	**ωB97XD**
PF1	9.5	3.1	3.2	4.0	5.6	3.3	8.2	16.4
PF2	17.1	0.4	6.7	8.4	7.7	0.8	14.1	18.8
PF3	-	13.6	15.9	17.4	17.3	16.1	19.4	26.7
PF4	13.3	12.5	15.8	17.0	15.9	16.1	20.2	22.2
PF5	20.3	8.5	9.6	9.9	10.1	6.1	18.8	20.9

PF6	-	15.0	18.6	19.2	19.1	19.2	20.7	23.9
PF7	17.0	8.3	9.6	18.8	13.7	6.4	22.3	24.8
PF8	20.8	11.9	18.3	20.7	18.2	22.8	23.5	26.7

a. Ref. [40] (MP2/def2-TZVP and B3LYP/def2-TZVP/COSMO).

Except for PF1 and PF2, ground-state D-E dihedral angles predicted by DFT methods in gas-phase are close to those calculated at the MP2/def2-TZVP level of theory level by Siddique and coworkers,[40] as shown in Table 1. In comparison to B3LYP/def2-TZVP/COSMO in acetonitrile, again PF1 and PF2 present the larger discrepancies in dihedral angles. The slight differences between the two B3LYP set of results is due to differences in the basis set and solvation model employed in the calculations reported by the Siddique team. The comparison between DFT results presented in Table 1 reveals that the TPSSh and ωB97XD functionals yield the most discrepant values for this geometric parameter. In essence, TPSSh results in tighter dihedral angles and more coplanar geometries, while ωB97XD results in the largest ones. Nevertheless, the variation of D-E dihedral angle was found to be lower than 20° when comparing both methods, showing a good agreement between them. Such small variations do not produce significant changes in photophysical properties, such as S_1 and T_1 energies, given that the PF^+ compounds present a π-delocalized electronic system over almost the entire molecule, which is one aspect well described by DFT approaches.[54]

Although range-separated functionals present the same percentage of Hartree-Fock exchange, they provided results with significant discrepancy between them. This could be due to the differences in the range-separated parameter (ω), but also to their different mathematical formulations. For instance, the ωB97XD functional presents a dispersion term while CAM-B3LYP takes into account the smoothness of the coulombic potential curve. When compared to other functionals, ωB97XD provides the largest differences in terms of geometry, which is a consequence of the dispersion terms included in this functional. As it improves the description of the unbound intramolecular interactions, the insertion of dispersion terms yields significant changes in molecular conformations.[55,56] In the case of pyranoflavylium cations, the interaction between the π clouds located in the center and in the B and E rings leads to the discrepancy observed for this functional.

This comparative analysis suggests that the increase in the percentage of Hartree-Fock exchange (HF) among the global-hybrid functionals as well as the type of functional

has a small influence on the geometry optimization, since they yield very similar geometries. So, these DFT functionals present a reasonable and consistent performance to optimize the geometries of pyranoflavylium cations.

Electronic absorption spectra

The mechanism of the most common applications of organic chromophores as photosensitizers, e.g. PDT, starts from the interaction between visible light and the chromophore. In the S_1 excited state, the chromophore is able to promote photophysical processes of interest, such as fluorescence and intersystem crossing[7]. For photodynamic applications, the position of the spectroscopic absorption bands is important as it determines the ability to photoexcite the molecules given the limited tissue-depth penetration of light. In addition, the energy initially absorbed from light determines the initial excited-state population thus impacting the subsequent decay processes.

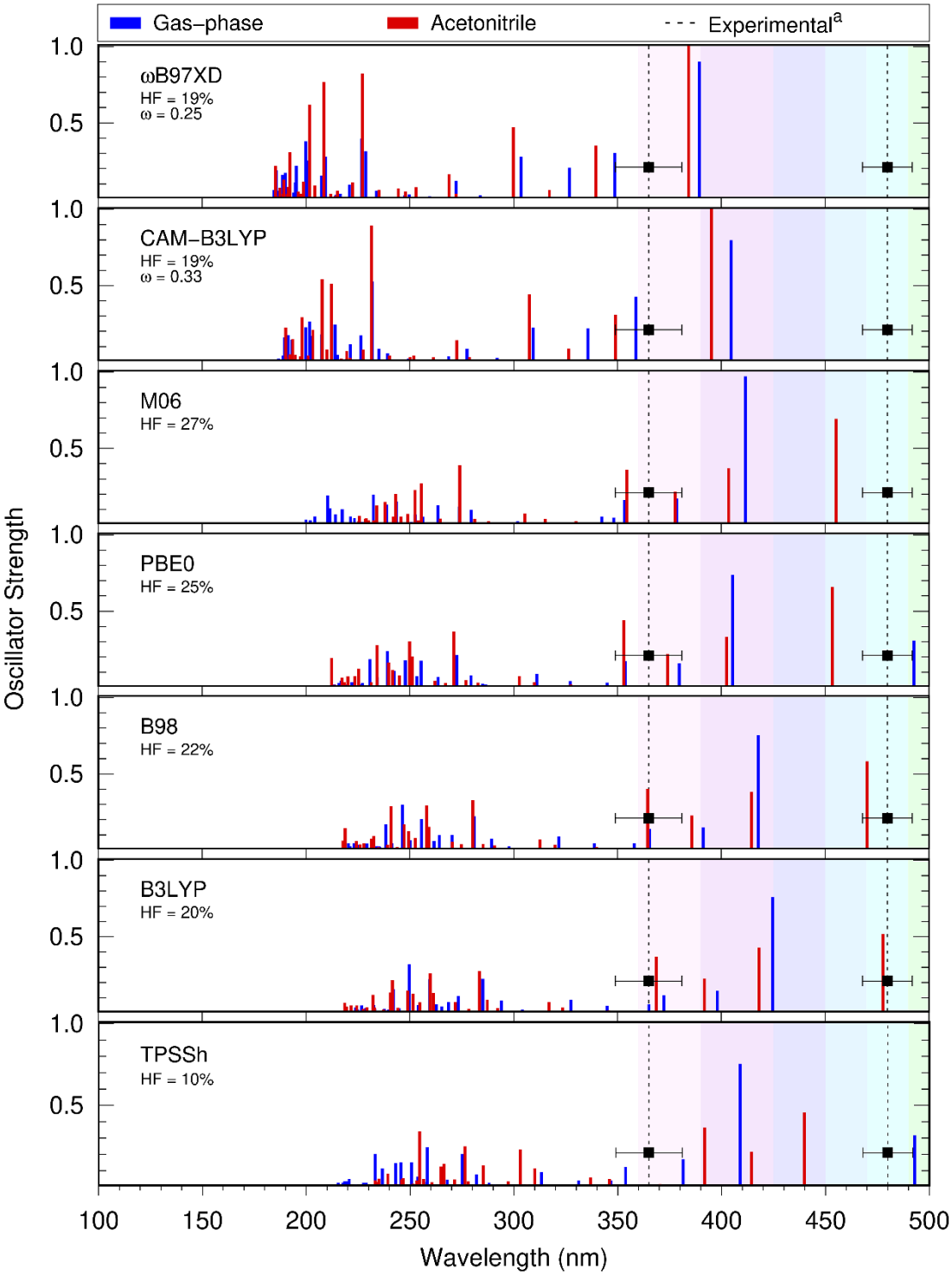

Figure 2: Electronic absorption spectra calculated for PF3 by different TD-DFT functionals in gas-phase and in acetonitrile. UV-visible spectral region is represented by transparent colors in the graphs. [a.] Ref. [4].

According to Figures SI4-SI11 (support information), different DFT functionals provide similar spectral profiles for each pyranoflavylium cation, except for compound

PF3, for which the largest variation is obtained with global-hybrid functionals (Figure 2). The increasing HF exchange percentage significantly modulates the position of all spectra, the higher this percentage the higher the displacement towards the blue spectral region. In other words, the increase of the HF exchange leads to an hypsochromic shift in all spectra. Additionally, the separation of the HF exchange action range by the ω parameter also intensifies that effect for all molecules.

Once acetonitrile solvation is included, the first (S_1) and second (S_2) excited states shift toward the red spectral region. In addition, increases in the oscillator strengths of the S_2 and S_3 states indicate that acetonitrile favors the initial population of these states. In contrast, all other absorption lines experience an hypsochromic shift in the acetonitrile environment. Nevertheless, several excited states are high in energy, beyond the UV-visible region (< 250 nm), so they are not relevant for visible-light induced photodynamic processes, and therefore will not be discussed further in this work. In Figures 3 and 4, the energy and character (major configuration) of the first seven excited states located near the UV and visible spectral regions are presented.

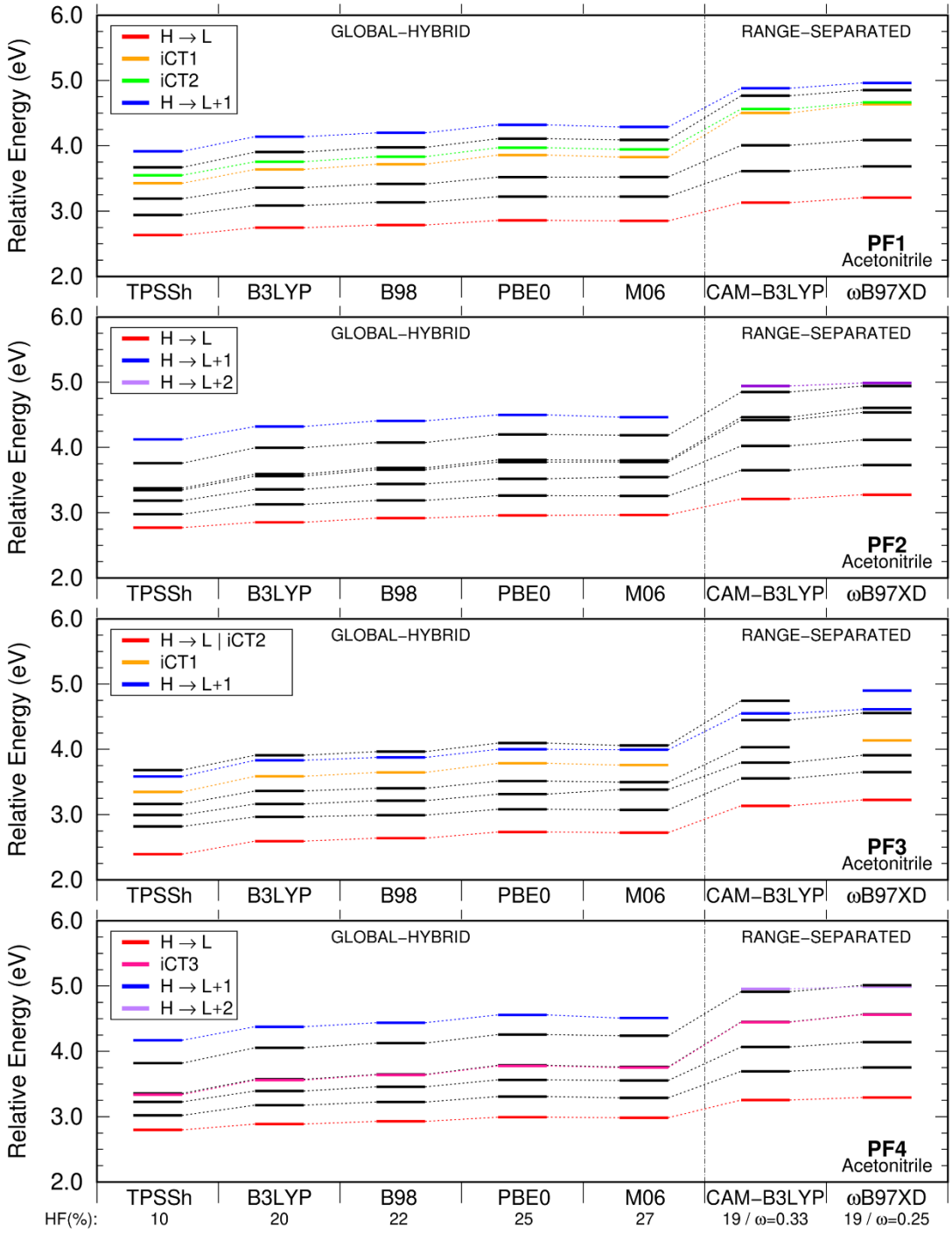

Figure 3: Singlet excited states in the UV-visible spectral range calculated using different DFT functionals in acetonitrile for compounds PF1-PF4. Intramolecular charge transfer states, iCTn n=1,2 and 3, from B, E and B+E rings are highlighted in yellow, green and pink colors, respectively. H = HOMO and L = LUMO

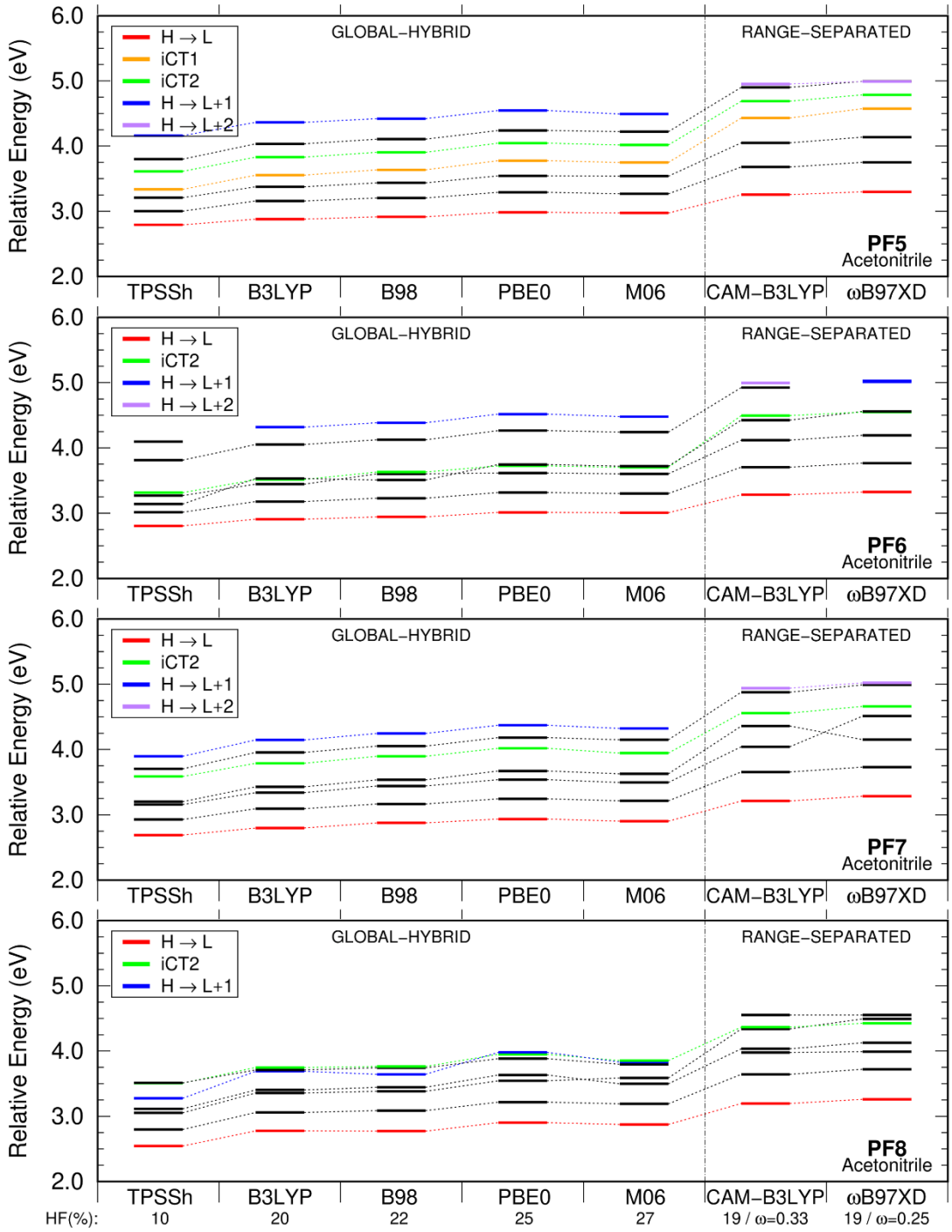

Figure 4: Singlet excited states in the UV-visible spectral range calculated using different DFT functionals in acetonitrile for compounds PF5-PF8. Intramolecular charge transfer states (iCTn n=1,2,3) from B, E and B+E rings are highlighted in yellow, green and pink colors, respectively. H = HOMO and L = LUMO

Except for PF6 and PF8, for which several inversions of state order occurred, global-hybrid functionals have predicted the same order and character of the excited states (Figure 3 and 4). In contrast, range-separated functionals yield a different order and nature

of the excited states when compared to global-hybrids, except for PF1. In addition, RS functionals predicted all excited states at higher energies than GH functionals. As can be observed, the energy of the excited states is related to their electronic configurations, which is defined by the molecular orbitals energies and character and electronic transitions.

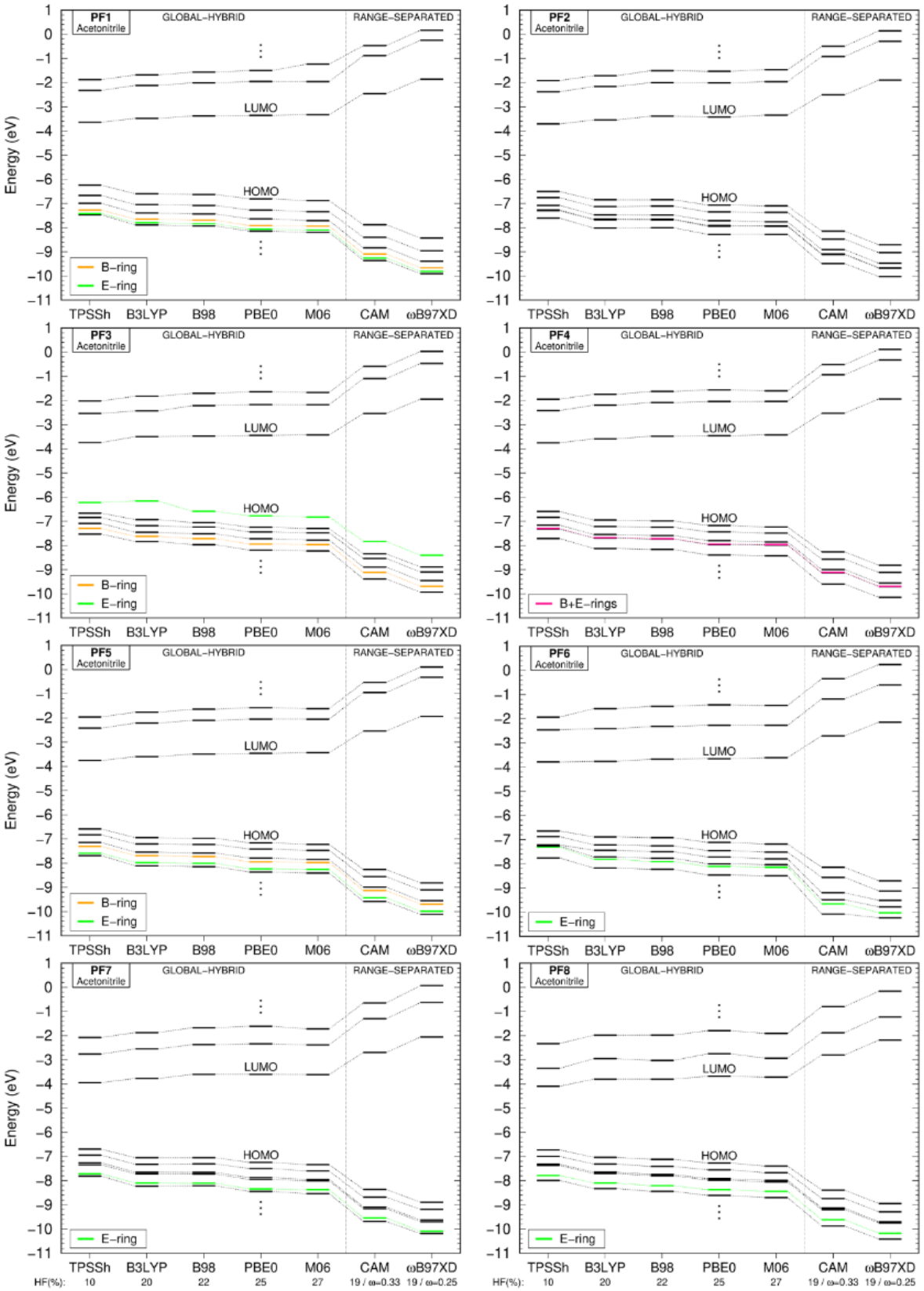

Figure 5: Molecular orbital energies calculated by different DFT functionals in the acetonitrile environment for PF^{+} compounds. Orbitals localized on B, E and B+E rings

are highlighted in yellow, green and pink colors, respectively. Vertical dots correspond to other orbitals

In Figure 5, the molecular orbital energies calculated for the pyranoflavylium cations are reported. As the percent of HF exchange increases, the occupied orbitals decrease in energy and the virtual orbitals experience a slight increase, which increases the gap, as expected with increasing HF percentage. The separation of the action range of the HF exchange, defined by the parameter ω, intensifies this effect, so that a smaller ω leads to a greater splitting of molecular orbitals, consequently increasing the HOMO-LUMO gap (Figure 5).

The charge transfer states are characterized as an electronic density redistribution along the molecule, for which B and/or E rings are responsible for the injection of density on the central part of the molecule, rings ACD. Charge transfer states are known as "dark states", once they do not present photoabsorption neither photoemission band in the visible spectrum. In the context of DFT simulations, iCT states are associated to null or very low oscillation strength, as can be observed in the obtained spectra (Figures SI4-SI11). All the compounds present charge transfer from E ring (iCT2), except for PF2, for which this transition may be suppressed since methyl group has a weak mesomeric effect. For compounds PF1, PF3 and PF5, two orbitals were found to be located on the B and E rings (Figures SI12, SI14 and SI16), which give origin to two intramolecular charge transfer states, respectively named iCT1 and iCT2 (Figures 3 and 4). On the other hand, only the orbital localized on the E ring appears in compounds PF6, PF7 and PF8 (Figures SI17, SI18, SI19), which gives rise to the iCT2 state. For compound PF4, a unique charge transfer state was also found (iCT3), in which both B and E rings inject electronic density on the molecular central region. This happens as a consequence of the ring's symmetry condition of this derivative.

According to the molecular orbital energy diagrams (Figure 5), their surfaces presented in Figures SI12-SI19 (support information) and their transition weights presented in Figure SI20 (support information), the nature of the excited states varies depending on the compound. Nonetheless, for all molecules the first excited state (S_1) was unanimously predicted to be mostly characterized by the HOMO→LUMO transition. HOMO→LUMO+1 and HOMO→LUMO+2 states are also highlighted in the graphs shown in Figures 3 and 4 to better visualize their energetic ordering. Once the energy

difference between LUMO+1 and LUMO is higher than that between HOMO-1 and HOMO, the HOMO→LUMO+1 state is higher in energy, and it is not the second excited state as it is for other organic molecules. Specially for range-separated functionals, HOMO→LUMO+2 also appears as the majority configuration of the S_7 state. Despite all the energy variations among DFT functionals, changes in the order of molecular orbitals have not been found, which also supports the consistency of DFT results when predicting the electronic structure of PF^+ compounds.

Fluorescence and Phosphorescence

In Figures SI21-SI23 (support information), the experimental and theoretical fluorescence and phosphorescence energies of the PF^+ under investigation are reported. These energies calculated from global-hybrid functionals results do not display remarkable variations. Although fluorescence energies present non-uniform values when calculated by hybrid functionals in gas-phase, those energies are very close to experimental data when calculated in the isopropanol environment. On the other hand, range-separated functionals yield in the greatest discrepancies against the considered references, even though they are small differences. The results reported in Figure SI21-SI23 (support information) averaged over functional types are summarized in Figure 6. The phosphorescence energies calculated for all compounds and by all density methods are higher enough to generate singlet oxygen (~ 0.99 eV)[57], which suggests potential to be used in photodynamic therapy.

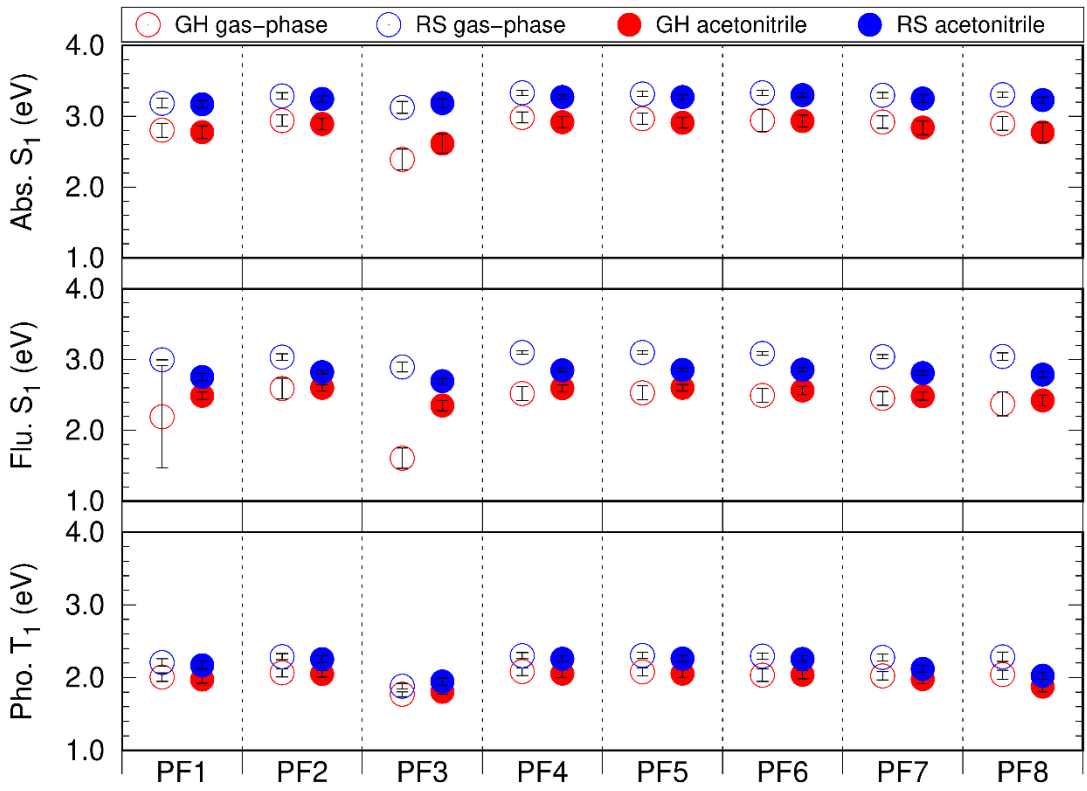

Figure 6: Average energies and standard deviation for vertical S_1 absorption, vertical S_1 emission and vertical T_1 emission calculated by global-hybrid (GH) and range-separated (RS) functional in gas-phase and in acetonitrile solution for PF^+ compounds

Statistics

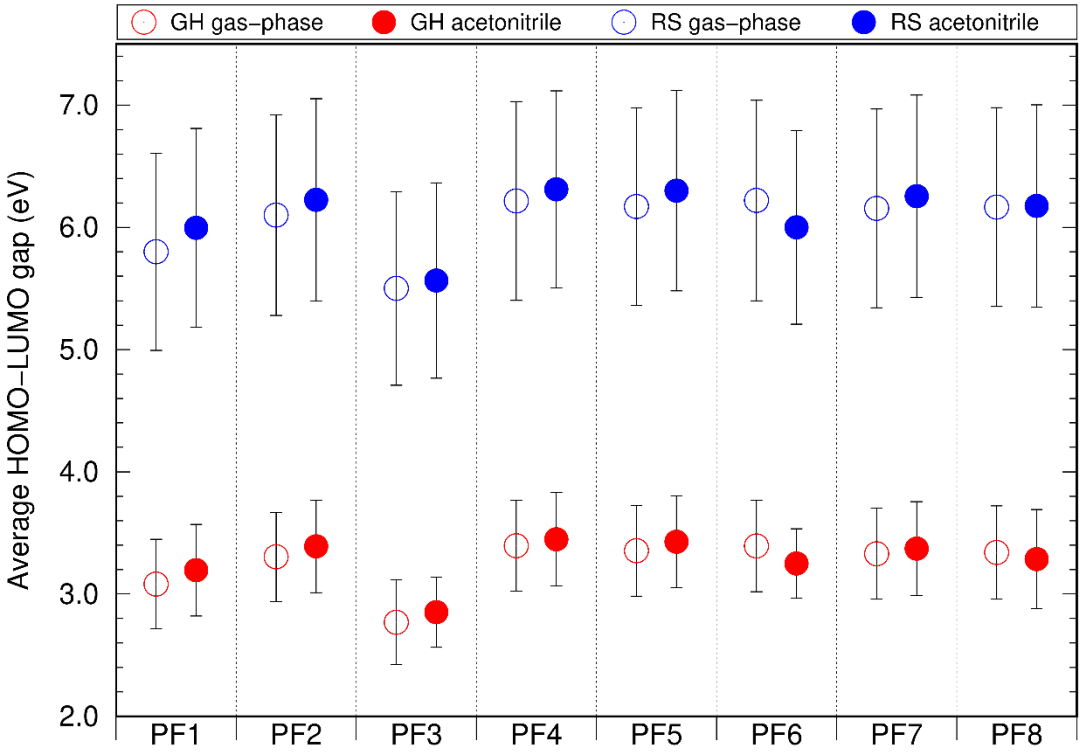

Figure 7: Average and standard deviation for HOMO-LUMO gaps calculated by global-hybrids (GH) and range-separated (RS) functionals in gas-phase and in acetonitrile solution for PF^+ compounds.

According to Figure 7, although solvation has not significantly affected the energy difference between orbitals, HOMO-LUMO gaps were found to be very discrepant when comparing both types of DFT functionals. On average, range-separated functionals yield systematically higher HOMO-LUMO gaps than global-hybrid functionals, being approximately 3.0 eV higher.

On average, absorption, fluorescence, and phosphorescence energies were consistently predicted by DFT methods, as shown in Figure 6. According to standard deviation, S_1 absorption for PF1 in gas-phase was found to be the most spread obtained data, which is due to the discrepant E ring conformation obtained for the first singlet excited state by global-hybrids (Figure SI21). In the cases of S_1 absorption and T_1 emission, the inclusion of solvation does not significantly change their energies, except for PF1 and PF3. However, the S_1 emission was considerably affected by solvation, with averaged fluorescence energies obtained using RS functionals decreasing while GH functionals display increases. Again, PF3 presented the most discrepant values for those photophysical processes most likely due to the presence of the naphthyl group, which is

highly saturated and causes an extension of the π-conjugated system which slightly changes the energy of the photophysical processes in question.

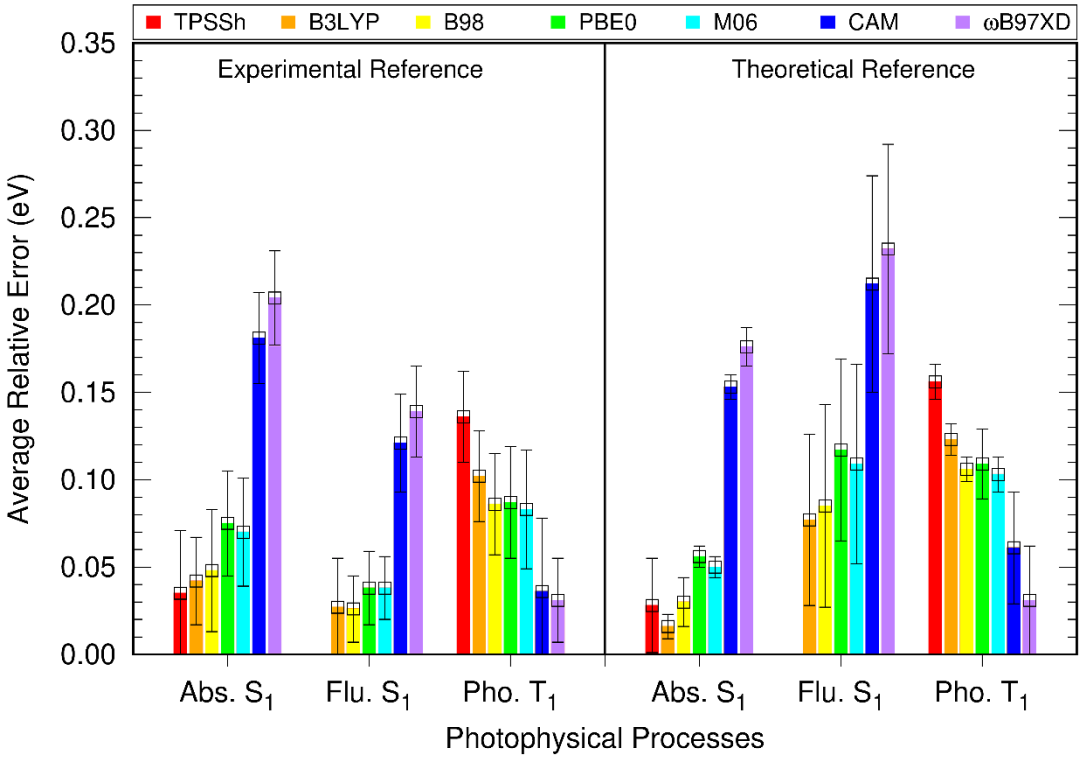

Figure 8: Average relative errors and standard deviation between S_1 absorption, S_1 emission and T_1 emission energies calculated for PF^+ compounds compared to experimental[4] and theoretical (ADC(2)/def2-TZVP/COSMO)[40] reference data. Note that TPSSh was not available for S_1 fluorescence.

The mean relative error and standard deviation calculated using the data obtained for all PF^+ compounds against experimental and theoretical references are shown in Figure 8. For the S_1 absorption process (Abs. S_1), the errors found for DFT functionals were smaller when using theoretical data as the reference. This means that (TD)DFT results are closer to theoretical references than to experimental data. Range-separated functionals yield the highest errors for absorption, considering both references, the largest being 0.20 eV when ωB97XD is compared to experimental values. On the other hand, the TPSSh and B3LYP functionals present the lowest errors, 0.035 eV and 0.016 eV, when compared to experimental and theoretical references, respectively, showing an excellent performance. The standard deviation of GH and RS functionals does not overlap, which certifies that they provide statistically significant differences between them when

predicting absorption energies. In comparison to experimental data, the standard deviations of global-hybrid functionals present a large overlap, which indicates no significant difference among those functionals. Considering the theoretical reference for Abs S_1, except for TPSSh, standard deviations for all DFT functionals are quite small, and they show minor or negligible overlaps between them. B3LYP and M06 present the smallest deviations, 0.025 eV (experimental reference) and 0.006 eV (theoretical reference), respectively. On the other hand, TPSSh displays the largest deviations among all the functionals employed, being 0.036 eV and 0.027 eV with respect to experimental and theoretical reference, respectively. So, for hybrids with about 20% of Hartree-Fock exchange, there is a better compromise in predicting the gap and, consequently, the whole spectra for these compounds.

In contrast to absorption, the errors for fluorescence from S_1 (Flu. S_1) were found to be smaller when compared to experiments than to theoretical reference data. In addition, RS functionals again presented higher errors than GH functionals for both references, the largest being 0.258 eV (theoretical reference) for ωB97XD while the smallest error was obtained for B3LYP, 0.016 eV (experimental reference). The greater deviations found in the comparison with theoretical references demonstrate that the DFT results are more spread around the ADC(2)/def2-TZVP/COSMO results than in relation to the experimental data. In other words, DFT results for PF^+ molecules seem to be more accurate but also more robust than ADC(2) ones. Again, non-overlapping standard deviation of GH and RS results suggest that their differences in performance are statically significant. On the other hand, such standard deviations in turn indicate no statistically significant difference among the GH and RS group of functionals. This result supports the consistency among DFT methods when estimating photophysical molecular properties.

The errors obtained for phosphorescence (Pho. T_1) showed a different trend when compared to the other photophysical processes discussed previously. According to Figure 6, ωB97XD leads to the best agreement with experimental and theoretical references, with remarkably small errors equal to 0.031 eV and 0.033 eV, respectively. In comparison to GH functionals, the increase in HOMO-LUMO gaps found for RS functionals (Figure 5) lead to an elevation of the first triplet excited state energy, given that LUMO is also half-filled in this state. This H-L gap also explains the increase of the fluorescence energy calculated from RS functionals. Among GH functionals, the largest error was found for the TPSSh, 0.158 eV (theoretical reference), and the smallest was found for M06, 0.103

eV (experimental data). The standard deviations found for GH functionals mostly overlap, except for TPSSh, which again demonstrates no significant difference between the performance of these functionals.

CONCLUSIONS

In this article, a benchmark on the performance of density functional theory methods on describing photophysical properties of eight pyranoflavylium cations is reported. DFT predictions were compared to experimental as well as previously reported theoretical data. Structural analysis of the predicted geometries for ground and excited singlet and triplet states indicates that the functional assessed led to reliable results comparable to those obtained by the MP2 methodology, especially if dispersion corrections are included. On the other hand, the data presented in this article show that different flavors of global-hybrid functionals present very similar results in terms of molecular orbitals and transition energies for photophysical processes like absorption, fluorescence and phosphorescence. RS functionals, in turn, lead to higher HOMO-LUMO gaps and higher energies for these photophysical processes compared to GH functionals.

DFT functionals also led to similar excited states in terms of their nature, predicting several intramolecular charge transfer states, in which the injection of electronic density from E ring (substituent group R) occurs for all molecules, except for PF2. On the other hand, charge transfer starting from the B ring was obtained only for PF1, PF3 and PF5 compounds. As expected, range-separated functionals led to higher energies for these charge transfer states, but remarkable the state ordering remained like that found with global-hybrids.

Statistical analysis of the obtained results, based on comparison with theoretical and experimental references, has shown that GH functionals lead to more accurate results for S_1 absorption and S_1 emission energies, while RS functionals yielded more accurate results for T_1 emission. B3LYP presented the most satisfactory results for the description of the processes involving S_1, while ωB97XD has shown the best performance for phosphorescence. Therefore, functionals with high percentages of Hartree-Fock exchange are necessary to study the main photophysical properties of this important class of compounds, and, depending on the target property (mainly those related to triplet states), it might be necessary to adopt range-separated approaches.

ACKNOWLEGDEMENTS

The author J. R. S. thanks the São Paulo State Research Support Foundation (FAPESP) for the grants number 2018/25576-6 and 2021/09841-4. Y. A. A. also thanks the São Paulo State Research Support Foundation (FAPESP) for the grant number and 2017/21199-0. P. H.-M. thanks the Brazilian National Council for Science and Technological Development (CNPq) for the grant 306585/2019-7. C. C. acknowledges financial support from the State Research Agency/Spanish Ministry of Science and Innovation (AEI/10.13039/501100011033; grants MDM-2017-0767, PID2020-115812GB-I00 and CEX2021-001202-M). This study was also financed in part by the Coordenação de Aperfeiçoamento de Pessoal de Nível Superior - Brasil (CAPES) – Finance Code 001.

BIBLIOGRAPHY

1. Freitas, A. A., Silva, C. P., Silva, G. T. M., Maçanita, A. L. & Quina, F. H. From vine to wine: Photophysics of a pyranoflavylium analog of red wine pyranoanthocyanins. *Pure Appl. Chem.* **89**, 1761–1767 (2017).
2. Freitas, A. A., Silva, C. P., Silva, G. T. M., Maçanita, A. L. & Quina, F. H. Ground- and Excited-State Acidity of Analogs of Red Wine Pyranoanthocyanins,. *Photochem. Photobiol.* **94**, 1086–1091 (2018).
3. Martins, L. M. O. S. *et al.* Red Wine Inspired Chromophores as Photodynamic Therapy Sensitizers1. *Photochem. Photobiol.* (2022) doi:10.1111/php.13682.
4. Silva, G. T. M. *et al.* Triplet Excited States and Singlet Oxygen Production by Analogs of Red Wine Pyranoanthocyanins. *Photochem. Photobiol.* **95**, 176–182 (2019).
5. Bacellar, I. O. L. *et al.* Photosensitized Membrane Permeabilization Requires Contact-Dependent Reactions between Photosensitizer and Lipids. *J. Am. Chem. Soc.* **140**, 9606–9615 (2018).
6. Baptista, M. S., Cadet, J., Greer, A. & Thomas, A. H. Photosensitization Reactions of Biomolecules: Definition, Targets and Mechanisms. *Photochem. Photobiol.* **97**, 1456–1483 (2021).
7. Turro, N. J., Ramamurthy, V. & Scaiano, J. C. *Modern Molecular Photochemistry of Organic Molecules*. (University Science Books, 2010).

8. Baptista, M. S. *et al.* Type I and Type II Photosensitized Oxidation Reactions: Guidelines and Mechanistic Pathways. *Photochem. Photobiol.* **93**, 912–919 (2017).
9. Laustriat, G. Molecular mechanisms of photosensitization. *Biochimie* **68**, 771–778 (1986).
10. Ochsner, M. Photophysical and photobiological processes in the photodynamic therapy of tumours. *J. Photochem. Photobiol. B Biol.* **39**, 1–18 (1997).
11. Tasso, T. T. *et al.* Photobleaching Efficiency Parallels the Enhancement of Membrane Damage for Porphyrazine Photosensitizers. *J. Am. Chem. Soc.* **141**, 15547–15556 (2019).
12. Ortel, B., Shea, C. & Calzavara-Pinton, P. Molecular mechanism of photodynamic therapy. *Front. Biosci.* **14**, 4157–4172 (2009).
13. Aono, C. M., Coutinho-Neto, M. D., Miotto, R. & Homem-De-Mello, P. CAHM1: A Theory-Based Proposal for a New DSSC D-A-π-A Dye. *J. Phys. Chem. C* **122**, 27256–27262 (2018).
14. Machado, N., Carvalho, B. G., Téllez Soto, C. A., Martin, A. A. & Favero, P. P. DFT application for chlorin derivatives photosensitizer drugs modeling. *Spectrochim. Acta - Part A Mol. Biomol. Spectrosc.* **195**, 68–74 (2018).
15. De Carvalho, F., Coutinho Neto, M. D., Bartoloni, F. H. & Homem-de-Mello, P. Density functional theory applied to excited state intramolecular proton transfer in imidazole-, oxazole-, and thiazole-based systems. *Molecules* **23**, (2018).
16. Hehn, A. S. *et al.* Excited-State Properties for Extended Systems: Efficient Hybrid Density Functional Methods. *J. Chem. Theory Comput.* **18**, 4186–4202 (2022).
17. Nguyen, V. N., Yan, Y., Zhao, J. & Yoon, J. Heavy-Atom-Free Photosensitizers: From Molecular Design to Applications in the Photodynamic Therapy of Cancer. *Acc. Chem. Res.* **54**, 207–220 (2021).
18. Sun, X. W., Peng, L. Y., Gao, Y. J., Ye, J. T. & Cui, G. Theoretical studies on excited-state properties and luminescence mechanism of a Carbene–Metal–Amide Au(I) complex with thermally activated delayed fluorescence. *J. Chinese Chem. Soc.* 1–9 (2022) doi:10.1002/jccs.202200193.
19. Tessaro, A. L. *et al.* Electronic structures and spectroscopic properties of benzoporphyrin protolytic species: A TD-DFT study. *Comput. Theor. Chem.* **1020**, 173–179 (2013).
20. Brémond, E., Savarese, M., Adamo, C. & Jacquemin, D. Accuracy of TD-DFT

Geometries: A Fresh Look. *J. Chem. Theory Comput.* **14**, 3715–3727 (2018).

21. Guido, C. A., Knecht, S., Kongsted, J. & Mennucci, B. Benchmarking time-dependent density functional theory for excited state geometries of organic molecules in gas-phase and in solution. *J. Chem. Theory Comput.* **9**, 2209–2220 (2013).
22. Jacquemin, D., Perpète, E. A., Ciofini, I. & Adamo, C. Assessment of functionals for TD-DFT calculations of singlet-triplet transitions. *J. Chem. Theory Comput.* **6**, 1532–1537 (2010).
23. Laurent, A. D., Adamo, C. & Jacquemin, D. Dye chemistry with time-dependent density functional theory. *Phys. Chem. Chem. Phys.* **16**, 14334–14356 (2014).
24. Jacquemin, D. & Adamo, C. Computational Molecular Electronic Spectroscopy with TD-DFT. in *Density-Functional Methods for Excited States. Topics in Current Chemistry* (eds. Ferré, N., Filatov, M. & Huix-Rotllant, M.) (Springer, 2015). doi:10.1007/128_2015_638.
25. Brémond, É. *et al.* Benchmarking Density Functionals on Structural Parameters of Small-/Medium-Sized Organic Molecules. *J. Chem. Theory Comput.* **12**, 459–465 (2016).
26. Grabarz, A. M. & Ośmiałowski, B. Benchmarking density functional approximations for excited-state properties of fluorescent dyes. *Molecules* **26**, 1–25 (2021).
27. Jacquemin, D., Wathelet, V., Perpète, E. A. & Adamo, C. Extensive TD-DFT benchmark: Singlet-excited states of organic molecules. *J. Chem. Theory Comput.* **5**, 2420–2435 (2009).
28. Jacquemin, D., Mennucci, B. & Adamo, C. Excited-state calculations with TD-DFT: From benchmarks to simulations in complex environments. *Phys. Chem. Chem. Phys.* **13**, 16987–16998 (2011).
29. De Souza, J. R., De Moraes, M. M. F., Aoto, Y. A. & Homem-De-Mello, P. Can one use the electronic absorption spectra of metalloporphyrins to benchmark electronic structure methods? A case study on the cobalt porphyrin. *Phys. Chem. Chem. Phys.* **22**, 23886–23898 (2020).
30. Goerigk, L. & Grimme, S. Assessment of TD-DFT methods and of various spin scaled CIS(D) and CC2 versions for the treatment of low-lying valence excitations of large organic dyes. *J. Chem. Phys.* **132**, 0–9 (2010).
31. Laurent, A. D. & Jacquemin, D. TD-DFT benchmarks: A review. *Int. J. Quantum*

Chem. **113**, 2019–2039 (2013).

32. Sarkar, R., Boggio-Pasqua, M., Loos, P. F. & Jacquemin, D. Benchmarking TD-DFT and Wave Function Methods for Oscillator Strengths and Excited-State Dipole Moments. *J. Chem. Theory Comput.* **17**, 1117–1132 (2021).
33. Silva-Junior, M. R., Schreiber, M., Sauer, S. P. A. & Thiel, W. Benchmarks for electronically excited states: Time-dependent density functional theory and density functional theory based multireference configuration interaction. *J. Chem. Phys.* **129**, (2008).
34. Zhao, Y. & Truhlar, D. G. The M06 suite of density functionals for main group thermochemistry, thermochemical kinetics, noncovalent interactions, excited states, and transition elements: Two new functionals and systematic testing of four M06-class functionals and 12 other function. *Theor. Chem. Acc.* **120**, 215–241 (2008).
35. Perdew, J. P., Kurth, S., Zupan, A. & Blaha, P. Accurate density functional with correct formal properties: A step beyond the generalized gradient approximation. *Phys. Rev. Lett.* **82**, 2544–2547 (1999).
36. Tao, J., Perdew, J. P., Staroverov, V. N. & Scuseria, G. E. Climbing the density functional ladder: Nonempirical meta–generalized gradient approximation designed for molecules and solids. *Phys. Rev. Lett.* **91**, 3–6 (2003).
37. Perdew, J. P., Tao, J., Staroverov, V. N. & Scuseria, G. E. Meta-generalized gradient approximation: Explanation of a realistic nonempirical density functional. *J. Chem. Phys.* **120**, 6898–6911 (2004).
38. Peverati, R. & Truhlar, D. G. Improving the accuracy of hybrid meta-GGA density functionals by range separation. *J. Phys. Chem. Lett.* **2**, 2810–2817 (2011).
39. Vydrov, O. A., Heyd, J., Krukau, A. V. & Scuseria, G. E. Importance of short-range versus long-range Hartree-Fock exchange for the performance of hybrid density functionals. *J. Chem. Phys.* **125**, (2006).
40. Siddique, F. *et al.* The electronic transitions of analogs of red wine pyranoanthocyanin pigments. *Photochem. Photobiol. Sci.* **18**, 45–53 (2019).
41. Frisch, M. J. *et al. Gaussian09, Revision D.01*. (Gaussian Inc., 2016).
42. Becke, A. D. Density-functional thermochemistry. III. The role of exact exchange. *J. Chem. Phys.* **98**, 5648–5652 (1993).
43. Schmider, H. L. & Becke, A. D. Optimized density functionals from the extended G2 test set. *J. Chem. Phys.* **108**, 9624–9631 (1998).

44. Adamo, C. & Barone, V. Toward reliable density functional methods without adjustable parameters: The PBE0 model. *J. Chem. Phys.* **110**, 6158–6170 (1999).
45. Yanai, T., Tew, D. P. & Handy, N. C. A new hybrid exchange-correlation functional using the Coulomb-attenuating method (CAM-B3LYP). *Chem. Phys. Lett.* **393**, 51–57 (2004).
46. Grimme, S., Antony, J., Ehrlich, S. & Krieg, H. A consistent and accurate ab initio parametrization of density functional dispersion correction (DFT-D) for the 94 elements H-Pu. *J. Chem. Phys.* **132**, (2010).
47. Schuchardt, K. L. *et al.* Basis set exchange: A community database for computational sciences. *J. Chem. Inf. Model.* **47**, 1045–1052 (2007).
48. Barone, V., Cossi, M. & Tomasi, J. Geometry optimization of molecular structures in solution by the polarizable continuum model. *J. Comput. Chem.* **19**, 404–417 (1998).
49. Cancès, E., Mennucci, B. & Tomasi, J. A new integral equation formalism for the polarizable continuum model: Theoretical background and applications to Isotropic and anisotropic dielectrics. *J. Chem. Phys.* **107**, 3032–3041 (1997).
50. Mennucci, B., Cancès, E. & Tomasi, J. Evaluation of solvent effects in isotropic and anisotropic dielectrics and in ionic solutions with a unified integral equation method: Theoretical bases, computational implementation, and numerical applications. *J. Phys. Chem. B* **101**, 10506–10517 (1997).
51. Mennucci, B. & Tomasi, J. Continuum solvation models: A new approach to the problem of solute's charge distribution and cavity boundaries. *J. Chem. Phys.* **106**, 5151–5158 (1997).
52. Tomasi, J., Mennucci, B. & Cancès, E. The IEF version of the PCM solvation method: An overview of a new method addressed to study molecular solutes at the QM ab initio level. *J. Mol. Struct. THEOCHEM* **464**, 211–226 (1999).
53. Silva, G. T. M. *et al.* Triplet Excited States and Singlet Oxygen Production by Analogs of Red Wine Pyranoanthocyanins. *Photochem. Photobiol.* 0–3 (2018) doi:10.1111/php.12973.
54. Rana, B., Beran, G. J. O. & Herbert, J. M. Correcting π-delocalisation errors in conformational energies using density-corrected DFT, with application to crystal polymorphs. *Mol. Phys.* 44–46 (2022) doi:10.1080/00268976.2022.2138789.
55. Minenkov, Y., Singstad, Å., Occhipinti, G. & Jensen, V. R. The accuracy of DFT-optimized geometries of functional transition metal compounds: A validation study

of catalysts for olefin metathesis and other reactions in the homogeneous phase. *Dalt. Trans.* **41**, 5526–5541 (2012).

56. Grimme, S. & Steinmetz, M. Effects of London dispersion correction in density functional theory on the structures of organic molecules in the gas phase. *Phys. Chem. Chem. Phys.* **15**, 16031–16042 (2013).

57. DeRosa, M. C. & Crutchley, R. J. Photosensitized singlet oxygen and its applications. *Coord. Chem. Rev.* **233**–**234**, 351–371 (2002).